

Extracting Matter Effects, Masses and Mixings at a Neutrino Factory*

M. FREUND^a, P. HUBER^b AND M. LINDNER^c

*Theoretische Physik, Physik Department, Technische Universität München,
James-Franck-Strasse, D-85748 Garching, Germany*

Abstract

We discuss and quantify different possibilities to determine matter effects, the value and the sign of Δm_{31}^2 , as well as the magnitude of $\sin^2 2\theta_{13}$ in very long baseline neutrino oscillation experiments. We study neutrino oscillation at a neutrino factory in the $\nu_\mu \rightarrow \nu_\mu$ disappearance and $\nu_e \rightarrow \nu_\mu$ appearance channels with and without muon charge identification. One possibility is to analyze the $\nu_e \rightarrow \nu_\mu$ appearance channels leading to wrong sign muon events, which requires however very good muon charge identification. Without charge identification it is still possible to operate the neutrino factory both with μ^- and μ^+ beams and to analyze the differences in the total neutrino event rate spectra. We show that this leads already to a quite good sensitivity, which may be important if right sign charge rejection capabilities are insufficient. With muon charge identification one can study the $\nu_\mu \rightarrow \nu_\mu$ disappearance and the $\nu_e \rightarrow \nu_\mu$ appearance channels independently. The best method is finally achieved by combining all available information of the $\nu_\mu \rightarrow \nu_\mu$ disappearance and $\nu_e \rightarrow \nu_\mu$ appearance channels with charge identification and we show the sensitivity which can be achieved.

*Work supported by "Sonderforschungsbereich 375 für Astro-Teilchenphysik" der Deutschen Forschungsgemeinschaft.

^aEmail: Martin.Freund@physik.tu-muenchen.de

^bEmail: Patrick.Huber@physik.tu-muenchen.de

^cEmail: Manfred.Lindner@physik.tu-muenchen.de

1 Introduction

Proposed neutrino factories [1, 2, 3, 4, 5] offer unique possibilities to improve the knowledge about neutrino masses, leptonic mixings and CP violation. The leptonic sector is not plagued by hadronic uncertainties such that vacuum neutrino oscillation allows to determine many parameters quite precisely. Vacuum neutrino oscillation is however only sensitive to mass squared differences thus the sign of Δm_{31}^2 can not be determined allowing therefore at the moment different scenarios for the ordering of mass eigenvalues. It has however been pointed out recently [6, 7, 8] that the sign of Δm_{31}^2 can be determined from the $\nu_e \rightarrow \nu_\mu$ and $\bar{\nu}_e \rightarrow \bar{\nu}_\mu$ appearance rates via matter effects [9] in very long baseline neutrino oscillation experiments at neutrino factories. We discuss and quantify in this paper further possibilities to determine the sign of Δm_{31}^2 via matter effects and $\sin^2 2\theta_{13}$ by considering the appearance channels and/or the $\nu_\mu \rightarrow \nu_\mu$ and $\bar{\nu}_\mu \rightarrow \bar{\nu}_\mu$ disappearance channels in different scenarios with and without muon charge identification. Altogether there are four possibilities. First, without charge identification one can not study wrong sign muon events (i.e. the appearance channels), but one can operate a neutrino factory already both with μ^- and μ^+ beams and analyze the differences in the combined muon neutrino and antineutrino event rate spectrum. This is useful if charge identification is not available or not operative in an initial stage of the experiment. We show that this leads already to a quite good sensitivity since the effects in the combined appearance and disappearance channels are for a baseline of 7332 km about the same size and go in the same direction. Next, with muon charge identification, one can study the $\nu_\mu \rightarrow \nu_\mu$ disappearance and the $\nu_e \rightarrow \nu_\mu$ appearance channels separately. For a baseline between 2800 km and 7332 km we find that the significance of these result is essentially unchanged compared to 7332 km. The point is that the total event rates decrease slower than the vacuum rates leading for a large range to a statistically constant result. We use therefore in this paper mostly a baseline of 7332 km since for this larger baseline there is further information in the disappearance channels. A third option would be to use the disappearance channel alone, this provides however not much extra information. Last, the best method is achieved with muon charge identification by combining all available information of the $\nu_\mu \rightarrow \nu_\mu$ disappearance and $\nu_e \rightarrow \nu_\mu$ appearance channels. We show for our baseline of 7332 km the sensitivity which can be achieved.

The basic effect which allows to extract the sign of Δm_{31}^2 comes from coherent forward scattering of electron neutrinos in matter which leads to effective masses and mixings different from vacuum. We will discuss in this paper a full three neutrino framework in the limit where the small solar mass splitting can be neglected in vacuum, i.e. $\Delta m_{21}^2 = 0$. This degeneracy is however destroyed in matter and we need therefore a full three neutrino description. The basic mechanism which allows the extraction of the sign of Δm^2 via matter effects can, however, already be seen in a simplified 2x2 picture with two mass eigenvalues m_i, m_j , $\Delta m^2 = m_j^2 - m_i^2$ and one mixing angle θ only.

One obtains then the well known relations for the parameters in matter

$$\Delta m_m^2 = \Delta m^2 C_{\pm} = \Delta m^2 \sqrt{\left(\frac{A}{\Delta m^2} \mp \cos 2\theta\right)^2 \pm \sin^2 2\theta} ; \quad \sin^2 2\theta_m = \sin^2 2\theta \cdot C_{\pm}^{-2} , \quad (1)$$

where the neutrino energy E enters via the matter term

$$A \equiv 2EV = \pm \frac{2\sqrt{2}G_F Y \rho E}{m_n} . \quad (2)$$

The sign of the matter term A is for electron neutrinos (antineutrinos) traveling inside the earth positive (negative) and leads thus to different corrections for neutrinos (C_+) and antineutrinos (C_-). Matter effects modify the 2x2 vacuum transition probabilities

$$P(\nu_i \rightarrow \nu_j) = \sin^2 2\theta \cdot \sin^2 \left(\frac{\Delta m^2 L}{E}\right) \quad \text{and} \quad P(\nu_{i,j} \rightarrow \nu_{i,j}) = 1 - P(\nu_i \rightarrow \nu_j) , \quad (3)$$

since in matter one must replace $\sin^2 2\theta \rightarrow \sin^2 2\theta_m$ and $\Delta m^2 \rightarrow \Delta m_m^2$. The matter corrections in eq. (1) depend for a given neutrino species (i.e. given A) clearly on the sign of Δm^2 allowing thus in principle an extraction of this sign. One could, for example, compare neutrinos with antineutrinos, since the matter corrections go then in opposite direction inducing an asymmetry. The biggest matter effects (and therefore the best sensitivity to the sign of Δm^2) occur when eq. (1) becomes “resonant” for

$$A = \Delta m^2 \cos 2\theta . \quad (4)$$

This condition can be fulfilled for a given sign of Δm^2 either for neutrinos or for antineutrinos at a specific resonance energy, but optimization will be more complicated in a real experiment with an energy spectrum and other free parameters. Nevertheless eq. (4) leads already to a rough approximation for a “optimal mean neutrino energy”. In earth eq. (4) gives for small θ , i.e. for $\cos 2\theta = 1$ roughly the relation

$$E_{opt} = 15 \text{ GeV} \left(\frac{\Delta m_{31}^2}{3.5 \times 10^{-3} \text{ eV}^2} \right) \cdot \left(\frac{2.8 \text{ g/cm}^3}{\rho} \right) , \quad (5)$$

i.e. an optimal energy of about 15 GeV in the crust of the earth with an average effective density $\langle \rho \rangle \simeq 2.8 \text{ g/cm}^3$ going down to about 10 GeV for paths crossing the earth at a distance of 7332 km with $\langle \rho \rangle \simeq 4.2 \text{ g/cm}^3$.

Our paper is organized as follows. First we develop in section 2 analytic expressions for neutrino oscillations in matter in a suitable approximation. In section 3 we describe the experimental framework on which our numerical results are based. Section 4 describes the effects of matter on the total rates and the used statistical methods are outlined in chapter 5. Section 6 contains our results on the sensitivity to the magnitude and sign of Δm_{31}^2 and for $\sin^2 2\theta_{13}$.

2 Analytic Description of three Neutrino Mixing in Matter

The mixing of three neutrinos can be described via

$$|\nu_l\rangle = \sum_{k=1}^3 U_{lk} |\nu_k\rangle, \quad l = e, \mu, \tau, \quad (6)$$

where $|\nu_l\rangle$ corresponds to the neutrino flavour state ν_l and $|\nu_k\rangle$ corresponds to the neutrino mass eigenstate ν_k with eigenvalues m_k , $m_k \neq m_j$, $k \neq j = 1, 2, 3$. U is a 3×3 unitary leptonic mixing matrix which we parameterize as

$$\begin{pmatrix} U_{e1} & U_{e2} & U_{e3} \\ U_{\mu 1} & U_{\mu 2} & U_{\mu 3} \\ U_{\tau 1} & U_{\tau 2} & U_{\tau 3} \end{pmatrix} = \begin{pmatrix} c_{12}c_{13} & s_{12}c_{13} & s_{13}e^{-i\delta} \\ -s_{12}c_{23} - c_{12}s_{23}s_{13}e^{i\delta} & c_{12}c_{23} - s_{12}s_{23}s_{13}e^{i\delta} & s_{23}c_{13} \\ s_{12}s_{23} - c_{12}c_{23}s_{13}e^{i\delta} & -c_{12}s_{23} - s_{12}c_{23}s_{13}e^{i\delta} & c_{23}c_{13} \end{pmatrix} \quad (7)$$

where $c_{ij} = \cos \theta_{ij}$ and $s_{ij} = \sin \theta_{ij}$. The mixing matrix contains in general further CP-violation phases which do not enter in neutrino oscillation and are therefore not specified [10]. The angles are assumed to be in the ranges $0 \leq \theta_{12}, \theta_{23}, \theta_{13} < \pi/2$, $0 \leq \delta < 2\pi$.

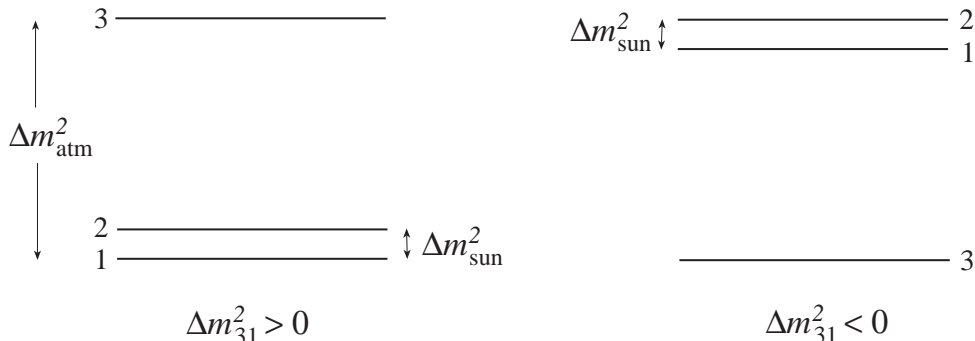


Figure 1: Two mass ordering schemes determined by the sign of Δm_{31}^2 .

The squared mass splittings $\Delta m^2 = m_j^2 - m_i^2$ show the hierarchy $\Delta m_{21}^2 \ll |\Delta m_{31}^2|$ as discussed in more detail below and allow for $\Delta m_{21}^2 \ll 10^{-4} \text{ eV}^2$, $E \geq 1 \text{ GeV}$ and $L \leq 10^4 \text{ km}$ the approximation where $\Delta m_{21}^2 = 0$ in vacuum. We have thus two almost degenerate mass eigenvalues and for $\Delta m_{31}^2 > 0$ ($\Delta m_{31}^2 < 0$) these almost degenerate eigenvalues m_1 and m_2 are lighter (heavier) than m_3 (see fig. 1). The usual oscillation formulas depend only on Δm_{31}^2 and it is thus impossible to discriminate between the two schemes. Matter effects and CP-violating effects can lift this degeneracy in future measurements in very long baseline experiments.

We can assume therefore for the following discussion that there is only one non-vanishing quadratic mass splitting $\Delta m_{32}^2 = \Delta m_{31}^2 = \Delta m^2$ in vacuum. To understand this case in matter we can write the mixing matrix eq. (7) as a sequence of rotations $U = R(\theta_{23}) \cdot R(\theta_{13}) \cdot R(\theta_{12})$ where the CP-phase δ is included in eq. (7) by a complex rotation in 13-subspace, i.e. by replacing $s_{13} \rightarrow s_{13}e^{-i\delta}$. Alternatively the CP-phase could be included

by making any of the three rotations complex. This becomes useful when we write the full Hamiltonian in matter with the help of U in flavour basis¹

$$\mathcal{H} = \frac{1}{2E} R(\theta_{23}) \left[R(\theta_{13}) \begin{pmatrix} 0 & 0 & 0 \\ 0 & 0 & 0 \\ 0 & 0 & \Delta m^2 \end{pmatrix} R(\theta_{13})^T + \begin{pmatrix} A & 0 & 0 \\ 0 & 0 & 0 \\ 0 & 0 & 0 \end{pmatrix} \right] R(\theta_{23})^T . \quad (8)$$

Here use has been made of the fact $R(\theta_{12})$, which operates in 12-subspace, drops out in the limit where $\Delta m_{21}^2 = 0$. Since we could use a convention where the CP-phase would be defined by a complex rotation in 12-subspace we can immediately see that the CP-phase drops out as well. Furthermore $R(\theta_{23})$ operates in the 23-subspace and commutes therefore with the matter term. We see that matter effects are confined in eq. (8) inside the square brackets, which implies that matter affects in the $\Delta m_{21}^2 = 0$ limit only the 13-subspace. We can readily use the standard two neutrino parameter mapping given in eqs. (1) for the 13-subspace and obtain in matter $\Delta m_{31,m}^2 = \Delta m^2 C_{\pm}$ and $\sin^2 2\theta_m = \sin^2 2\theta / C_{\pm}^2$, where $\Delta m^2 \equiv \Delta m_{31}^2$ enters into C_{\pm} defined in eq. 1. Note, however, that Δm_{32}^2 and Δm_{21}^2 become in matter in this way also energy dependent, namely

$$\Delta m_{32,m}^2 = \Delta m^2 C'_{\pm} = \frac{\Delta m^2 (C_{\pm} + 1) + A}{2} ; \quad \Delta m_{21,m}^2 = \Delta m^2 C''_{\pm} = \frac{\Delta m^2 (C_{\pm} - 1) - A}{2} . \quad (9)$$

An important consequence is that the mass degeneracy between the first two eigenvalues is destroyed in matter. Thus even if we can approximate $\Delta m_{21}^2 = 0$ in vacuum we need for oscillation in matter the full three neutrino oscillation formulae. The only simplification left is that one can set in the mixing matrix $\theta_{12} = 0$ and $\delta = 0$.

These matter induced parameter mappings must now be inserted into the oscillation formulae for three neutrinos. Defining as shorthands $D_{ab} = e^{-iE_a t} \delta_{ab}$, $J_{ij}^{lm} := U_{li} U_{lj}^* U_{mi}^* U_{mj}$ and $\Delta_{ij} := \Delta m_{ij}^2 L / 4E$ the transition probabilities $P(\nu_l \rightarrow \nu_m)$ from flavour l to flavour m in vacuum can be written as

$$P(\nu_l \rightarrow \nu_m) = |\langle l | U D U^+ | m \rangle|^2 = \delta_{lm} - 4 \sum_{i>j} \text{Re} J_{ij}^{lm} \sin^2 \Delta_{ij} - 2 \sum_{i>j} \text{Im} J_{ij}^{lm} \sin 2\Delta_{ij} . \quad (10)$$

As described above we can set in matter $\theta_{12} = 0$ and $\delta = 0$ resulting in

$$P(\nu_{\mu} \leftrightarrow \nu_e) = \sin^2 \theta_{23} \sin^2 2\theta_{13} \sin^2(\Delta_{31}) , \quad (11a)$$

$$P(\nu_{\mu} \leftrightarrow \nu_{\mu}) = 1 - \sin^2 2\theta_{23} \sin^2 \theta_{13} \sin^2(\Delta_{21}) - \sin^4 \theta_{23} \sin^2 2\theta_{13} \sin^2(\Delta_{31}) \\ - \sin^2 2\theta_{23} \cos^2 \theta_{13} \sin^2(\Delta_{32}) , \quad (11b)$$

$$P(\nu_{\mu} \leftrightarrow \nu_{\tau}) = \sin^2 2\theta_{23} \left[\sin^2 \theta_{13} \sin^2(\Delta_{21}) - \frac{1}{4} \sin^2 2\theta_{13} \sin^2(\Delta_{31}) \right. \\ \left. + \cos^2 \theta_{13} \sin^2(\Delta_{32}) \right] . \quad (11c)$$

To describe oscillation in matter we must insert into these formulae the parameter mappings discussed above, namely the shifted mass eigenvalues ($\Delta m_{31,m}^2 = \Delta m^2 C_{\pm}$ and eqs. (9))

¹A constant common neutrino mass can be separated leading to an overall phase.

and the shifted 13-mixing angle, $\sin^2 2\theta_{13,m} = \sin^2 2\theta_{13}/C_{\pm}^2$. Note that the relations for antineutrinos are only formally identical due to the opposite sign of the matter term A in eq. (1). In vacuum the relations (11a)–(11c) could be further simplified since the tight CHOOZ results [11] can be taken into account. For typically allowed Δm_{31}^2 values one has $\sin^2 2\theta_{13} \lesssim 0.1$, while this upper limit is less stringent for $1.0 \times 10^{-3} \text{ eV}^2 \leq |\Delta m_{31}^2| < 3.0 \times 10^{-3} \text{ eV}^2$ where values of $\sin^2 2\theta_{13} \simeq 0.2$ are allowed. Note however that the effective $\sin^2 2\theta_{13}$ in matter can be much bigger when the resonance condition is fulfilled such that further simplifications of eqs. (11a)–(11c) are potentially dangerous.

3 Experimental Framework

We use for our study a standard earth matter density profile [12, 13] and we will treat neutrino oscillations in earth by a constant density approximation along each neutrino path. The varying matter profile of the earth implies that the average density is still path dependent. It has been shown recently [14, 15] that this approximation works very well, while a constant density for all paths ignores even the mean density variations in the earth and has sizable errors². We avoid the core of the earth and take in our study distances up to 7332 km. We assume furthermore a neutrino factory which can operate with μ^- or μ^+ beams leading to $\nu_{\mu} + \bar{\nu}_e$ or $\bar{\nu}_{\mu} + \nu_e$ neutrino beams resulting from $N_{\mu\pm}$ muon decays. The detector with N_{kT} kilotons is assumed to be able to measure muons above an assumed threshold of 5 GeV [16] with an efficiency ϵ_{μ} . The muons may come from the dominant $\nu_{\mu} \rightarrow \nu_{\mu}$ disappearance channel or from the subdominant $\nu_e \rightarrow \nu_{\mu}$ appearance channel with or without charge identification. Muons coming from the subdominant $\nu_{\mu} \rightarrow \nu_{\tau}$ or $\nu_e \rightarrow \nu_{\tau}$ channels with the τ decaying subsequently to a muon should not be a problem, since they can be separated by kinematical means without losing too much muon detection efficiency [6]. The inclusion of various other potential backgrounds and detector properties will have some influence on the analysis, but with current understanding this would only result in moderate corrections. More detailed simulations of backgrounds are still in progress [16, 17, 18, 19]. Most limitations due to backgrounds and statistics can however be overcome by increasing the number of muon decays and/or the size of the detector. We do not include a detailed simulation of background effects at the moment.

For three neutrinos there is only room for two independent quadratic mass splittings while there are three different results for oscillation. Among these the LSND evidence [20] for oscillation is most controversial and we omit this result therefore in our analysis, while we take the atmospheric result (mostly from SuperKamiokande [21]) and the solar neutrino deficit (mostly from GALLEX [22]) as evidence for oscillation. These results can be studied in a simplified 2x2 oscillation picture where the mixing matrix contains only one mixing angle θ with the two flavour transition probabilities in vacuum given in eq. (3). The dominant atmospheric $\nu_{\mu} \leftrightarrow \nu_{\tau}$ oscillations imply in this picture a mass splitting [23]

$$10^{-3} \text{ eV}^2 \lesssim |\Delta m_{31}^2| \lesssim 8.0 \times 10^{-3} \text{ eV}^2 , \quad (12)$$

²Note also that care should be taken about the core of the earth. Either one should avoid paths passing the core or one should take core effects into account. Specific core effects become however small when the oscillation wavelength becomes bigger than the size of the core.

while the solar neutrino deficit leads to different solutions [24] for Δm_{21}^2 , all with $|\Delta m_{21}^2| \ll |\Delta m_{31}^2|$. These are the solar vacuum oscillation (VO) solution and the large and small mixing angle (LMA and SMA) solar MSW solutions. The above assignment implies thus that Δm_{31}^2 dominates the atmospheric $\nu_\mu \rightarrow \nu_\tau$ oscillation, while Δm_{21}^2 is most relevant for the VO, SMA MSW and LMA MSW solution of the solar neutrino problem. We will see that our study depends only on Δm_{31}^2 such that in a very good approximation Δm_{21}^2 can be set to zero. We use therefore as default initial parameters of our study

$$|\Delta m_{31}^2| = 3.5 \cdot 10^{-3} ; \quad |\Delta m_{21}^2| = 0 ; \quad \sin^2 2\theta_{23} = 1.0 \quad (13)$$

and we will discuss variations of these parameters within the allowed ranges.

The event rates of our results depend only on the combination $N_{\mu^\pm} N_{\text{kT}} \epsilon_\mu$ and we take for both polarities $N_{\mu^\pm} N_{\text{kT}} \epsilon_\mu = 2 \cdot 10^{21}$. This corresponds for example to a setup with $N_{\mu^+} = 2 \cdot 10^{20} \mu^+$ decays, $N_{\mu^-} = 2 \cdot 10^{20} \mu^-$ decays, an $N_{\text{kT}} = 10$ kt iron detector and a muon detection efficiency $\epsilon_\mu = 1$. Unless otherwise mentioned we use a baseline of $L = 7332$ km.

Our analysis is performed at the level of total and differential event rates. We include therefore the charged current neutrino cross sections per nucleon in the detector and the normalized $\nu_\mu + \bar{\nu}_e$ and $\bar{\nu}_\mu + \nu_e$ beam spectra g_{ν_i} of the neutrino factory [1]

$$\sigma_{\nu_\mu}(E) = 0.67 \cdot 10^{-38} E \text{ cm}^2/\text{GeV} , \quad \sigma_{\bar{\nu}_\mu}(E) = 0.34 \cdot 10^{-38} E \text{ cm}^2/\text{GeV} , \quad (14a)$$

$$g_{\nu_e}(x) = g_{\bar{\nu}_e}(x) = 12x^2(1-x) , \quad g_{\nu_\mu}(x) = g_{\bar{\nu}_\mu}(x) = 2x^2(3-2x) , \quad (14b)$$

where $x = E/E_\mu$. For a given number of useful muon decays N_{μ^\pm} , detector size N_{kT} , efficiency ϵ_μ one obtains for the channel "i" (where i stands for a proper index uniquely given by the polarity of the muon beam and the considered oscillation channel) the contributions to the differential event rates

$$\frac{dn_i}{dE} = \underbrace{\left[N_{\mu^i} N_{\text{kT}} \epsilon_\mu \frac{10^9 N_A}{m_\mu^2 \pi} \right]}_{\text{normalization}} \underbrace{\left[\frac{E_\mu}{L^2} g_i(E/E_\mu) \sigma_i(E) \right]}_{\text{flux}} \underbrace{\left[P_i(E) \right]}_{\text{oscillation}} \quad (15)$$

where $10^9 N_A$ is the number of nucleons per kiloton in the detector and P_i stands for the relevant oscillation probability in matter as discussed above. In cases where different channels contribute the total differential rates are given by the sum of all individual terms. Total rates are obtained by integrating these differential rates from the threshold at 5 GeV to the maximal possible neutrino energy E_μ .

To understand the event rates we look at the three terms in square brackets on the *rhs.* of eqs. (15). The first term contains overall factors which are constant in energy, which is only important for the proper event rate normalization. The second term is simply the product of flux times detection cross section which has to be folded with the third term, the oscillation probability in matter. The second term grows initially like E^3 and reaches a maximum before it goes to zero at $E = E_\mu$. An important feature of the second term is that the low energy part is not changed when the muon energy is increased. This implies in a good approximation that the increase in the total event rates by increasing E_μ comes essentially from the high energy tail of the spectrum only. This has also the important consequence that

experimental results for a lower muon beam energy $E'_\mu < E_\mu$ can in principle be obtained to a good approximation at higher energies by simply removing events with energies above E'_μ .

4 Total Rates

The analytic description above allows now an understanding of the event rates which we calculated numerically and which are presented below in fig. 2. To understand first the total disappearance rates without matter one must look at the folding of the vacuum oscillation probabilities with the flux factor in eq. (15). The oscillatory terms in the oscillation probabilities eqs. (10), namely the $\sin^2 \Delta_{ij}$ factors, depend then for fixed $\Delta m_{31}^2 = \Delta m^2$ only on E/L . The oscillatory behavior vanishes for $E/L \rightarrow \infty$ and the first maximum of the vacuum oscillation occurs for given L at an energy $E_1 = 2\Delta m^2 L/\pi$. This means that there will essentially be no effects of oscillation in the total disappearance rates when E_1 is much smaller than the neutrino energy E . Since the event rates are dominated by the maximum of the flux factor close to E_μ we can set $E \simeq E_\mu$ and find no oscillation effects when E_μ is much larger than E_1 . The overall rates will however still decrease with the muon energy E_μ according to the cross sections and fluxes approximately like E_μ^2 as long as E_μ is sufficiently larger than the muon threshold energy of 5 GeV. The first effects of vacuum oscillation show up for lower beam energies when $E \simeq E_\mu$ is decreased such that $E_\mu = \mathcal{O}(E_1)$. The oscillation becomes maximal for $E_\mu \simeq E_1$ while it vanishes again for $E_\mu \simeq E_1/2$. The effects of oscillation can be seen in the total rates as a dip in the overall E_μ^2 scaling. For lower beam energies there are in principle further dips due to all other oscillation maxima, but this is on our case below the threshold energy of 5 GeV.

In order to understand how matter effects influence the disappearance rates one must compare the matter “resonance energy” E_{opt} in eq. (5) at roughly 10 – 15 GeV with E_1 and $E_\mu \simeq E$. At neutrino energies which are not close to this resonance energy the mixing $\sin^2 2\theta_{13,m}$ approaches quickly its value in vacuum, which is small. One can see immediately from the Hamiltonian in eq. (8) that the dominant $\nu_\mu \rightarrow \nu_\tau$ oscillation decouples in the limit where $\sin^2 2\theta_{13} = 0$ from the matter effects coming from the first generation such that it is clear that matter effects should be rather localized around the resonance region³.

The total appearance rates are given for $E_\mu \gg E_1$ by the asymptotic behavior of eq. (11a) weighted with the flux. The increase in the rates with E_μ comes again predominantly from the increased flux at energies close to E_μ such that we need to look again in a good approximation at the asymptotic behaviour of $E_\mu^2 P(\nu_\mu \leftrightarrow \nu_e)$. Expanding $E_\mu^2 P(\nu_\mu \leftrightarrow \nu_e)$ in powers of $1/E$, and using the fact that $V \cdot L$ is numerically small, one finds for the asymptotic appearance rates for small $\sin^2 2\theta_{13}$

$$n \propto \sin^2 \theta_{23} \sin^2 2\theta_{13} (\Delta m^2)^2 L^2 \left(1 - \frac{(\Delta m^2)^2 L^4}{3E_\mu^2} \right) + \frac{4(\Delta m^2)^3 L^4 V}{3E_\mu}. \quad (16)$$

The result shows that the rates approach for $E_\mu \gg E_1$ in vacuum a constant which depends

³Note that the mass splittings Δm_{ij}^2 behave non-trivial in the high energy limit such that the asymptotic properties of eq. (11b) have to be evaluated carefully to reach the same conclusion.

only on even powers of Δm^2 . The leading corrections to this constant fall like $1/E_\mu^2$. Turning on matter effects leads in eq. (16) to the third term which falls only like $1/E_\mu$ and which depends on $(\Delta m^2)^3$, i.e. on the sign of Δm_{31}^2 . This induces in our case a matter dependent splitting in the appearance rates which is less localized in energy than the matter effects in the disappearance channels. There are thus significant effects even for beam energies which are somewhat away from the resonance energy. Note, however, that the discussion of effects is much more complicated for muon energies of the order or smaller than E_1 .

This understanding of matter effects can now be compared with the results of our full numerical calculations. The following figures for the total rates in the different oscillation channels assume $N_{\mu^\pm} N_{\text{KT}\epsilon_\mu} = 2 \cdot 10^{21}$, a fixed baseline of 7332 km, $|\Delta m_{31}^2| = 3.5 \cdot 10^{-3} \text{ eV}^2$, $\sin^2 2\theta_{23} = 1$ and different values of $\sin^2 2\theta_{13}$. If the muon beam energy is fixed then we use always $E_\mu = 20 \text{ GeV}$. Fig. 2 shows the $\nu_e \rightarrow \nu_\mu$ and $\bar{\nu}_e \rightarrow \bar{\nu}_\mu$ total appearance rates (dotted

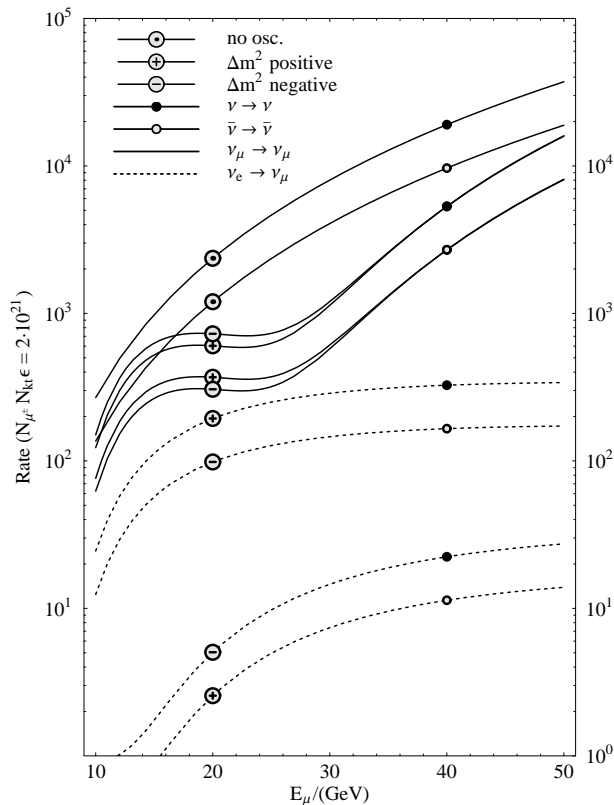


Figure 2: Muon appearance rates $\nu_e \rightarrow \nu_\mu$ and $\bar{\nu}_e \rightarrow \bar{\nu}_\mu$ (dotted) and muon disappearance rates $\nu_\mu \rightarrow \nu_\mu$ and $\bar{\nu}_\mu \rightarrow \bar{\nu}_\mu$ (solid) as a function of the muon beam energy for a baseline of 7332 km, $|\Delta m_{31}^2| = 3.5 \cdot 10^{-3} \text{ eV}^2$ and $\sin^2 2\theta_{13} = 0.1$. \oplus and \ominus indicate positive and negative mass squared difference, \odot indicates no oscillation rates. \bullet and \circ label the neutrino and the antineutrino channels.

lines) as well as the $\nu_\mu \rightarrow \nu_\mu$ and $\bar{\nu}_\mu \rightarrow \bar{\nu}_\mu$ disappearance rates (solid lines) on a logarithmic scale for maximal $\sin^2 2\theta_{13} = 0.1$. These rates are in agreement with the results obtained recently by Barger et. al [6]. The lines appear in pairs of neutrino (\bullet) and antineutrino (\circ) channels which differ roughly by a factor two coming from the cross sections eqs. (14).

Fig. 2 shows the cases with positive Δm_{31}^2 (\oplus), negative Δm_{31}^2 (\ominus) and no oscillation (\odot). The asymmetry between \oplus and \ominus in the appearance rates, which has been used to extract the sign of Δm_{31}^2 at smaller baseline [6, 25], is clearly visible. Note that there are also comparable matter effects in the disappearance channels at these large baselines, which appear only to be smaller due to the logarithmic scale. Fig. 2 shows clearly the important feature that the matter effects in the combined appearance and disappearance muon rates go for a neutrino factory with either $\nu_\mu + \bar{\nu}_e$ or $\bar{\nu}_\mu + \nu_e$ beams in the same direction. This opens an interesting possibility if muon charge identification is not available to separate the appearance channels (wrong sign muon events) from the disappearance channels (right sign muon events). It is then still possible to measure all muons, i.e. muons with both charges, or in other words the combination of the two oscillation channels, where matter effects add up. The resulting total muon rates of the combined channels are shown for both μ^- and μ^+ beams in fig. 3 on a linear scale for μ^- and μ^+ muon beams. The figure shows the sizable matter induced splittings in the total muon-neutrino rates ($\nu_\mu + \bar{\nu}_\mu$) for the mixing angles $\sin^2 2\theta_{13} = (0.1, 0.04, 0.01)$. The difference between the two signs of Δm_{31}^2

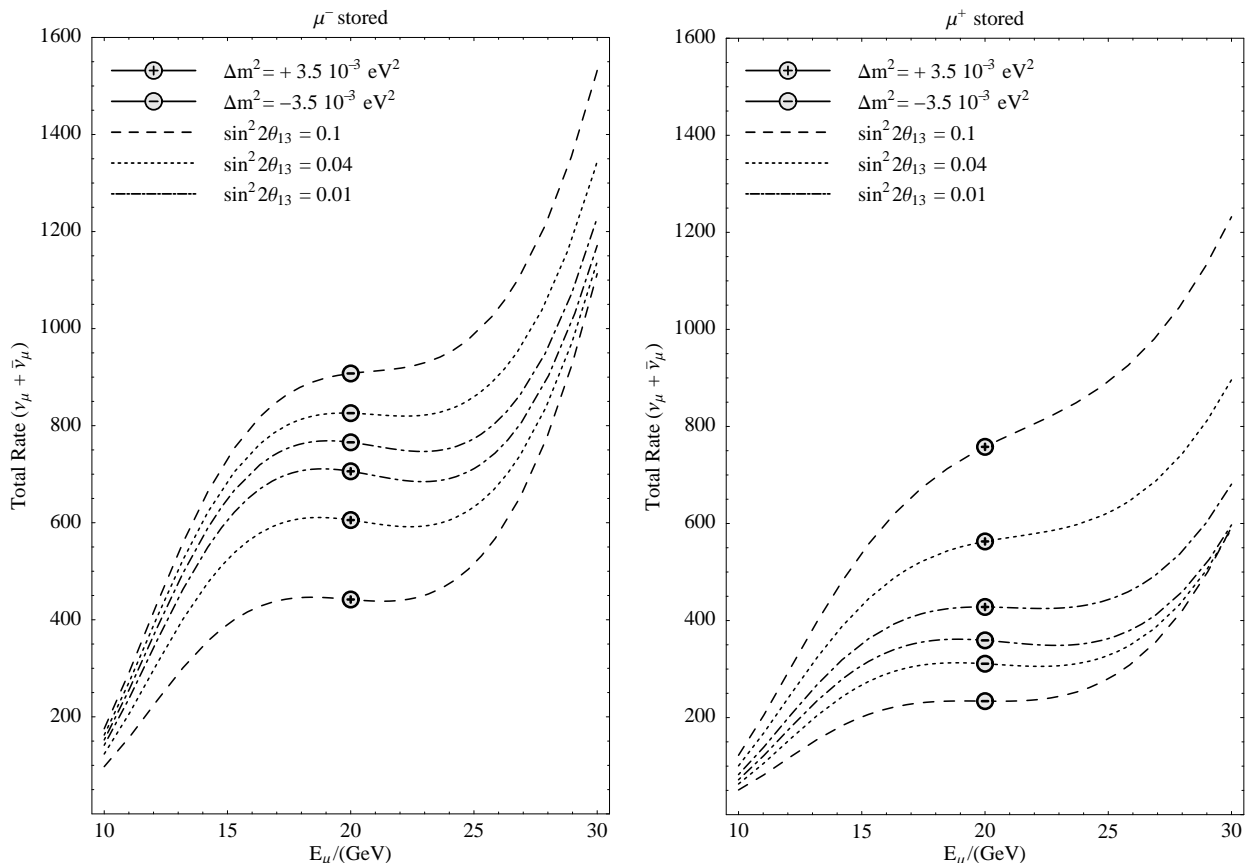


Figure 3: Total muon rates $\nu_\mu + \bar{\nu}_\mu$ (i.e. $\nu_\mu \rightarrow \nu_\mu$ combined with $\bar{\nu}_e \rightarrow \bar{\nu}_\mu$ and $\bar{\nu}_\mu \rightarrow \bar{\nu}_\mu$ combined with $\nu_e \rightarrow \nu_\mu$) as a function of the muon beam energy for a baseline of 7332 km, $|\Delta m_{31}^2| = 3.5 \cdot 10^{-3} \text{ eV}^2$ and $N_{\mu^\pm} N_{kT} \epsilon_\mu = 2 \cdot 10^{21}$ which corresponds typically to a 10 kt-year. The different line types stand for different mixing angles θ_{13} (see labels). \oplus and \ominus indicate positive and negative mass squared difference.

influences the total rates up to a factor two or more. The effect comes partly from the appearance rates and partly from the disappearance rates, but always from the resonant channel. This is for positive Δm_{31}^2 the neutrino component of the beam and for negative Δm_{31}^2 the antineutrino component. For μ^+ beams the interplay of the two channels is as follows⁴: For positive Δm_{31}^2 the $\nu_e \rightarrow \nu_\mu$ appearance channel is resonant leading to an enhancement of the combined rate, while matter corrections are moderate for the $\bar{\nu}_\mu \rightarrow \bar{\nu}_\mu$ disappearance channel. For negative Δm_{31}^2 , on the other side, the disappearance channel $\bar{\nu}_\mu \rightarrow \bar{\nu}_\mu$ shows a resonant transition of ν_μ to ν_e resulting in a suppression of the total $\nu_\mu + \bar{\nu}_\mu$ rate, while the $\nu_e \rightarrow \nu_\mu$ appearance rates are mostly unchanged. The combination of appearance and disappearance channels amplifies thus always the signal. This shows that an analysis of the combined appearance and disappearance channels is interesting and it may be especially important if the separation of right and wrong sign muon events is not available. Figure 4 shows the corresponding differential event rate spectrum of the $\nu_\mu + \bar{\nu}_\mu$ induced muon rate over twenty energy bins for a mixing angle $\sin^2 2\theta_{13} = 0.1$ (CHOOZ bound). We find that the different matter effects have no specific spectral features which

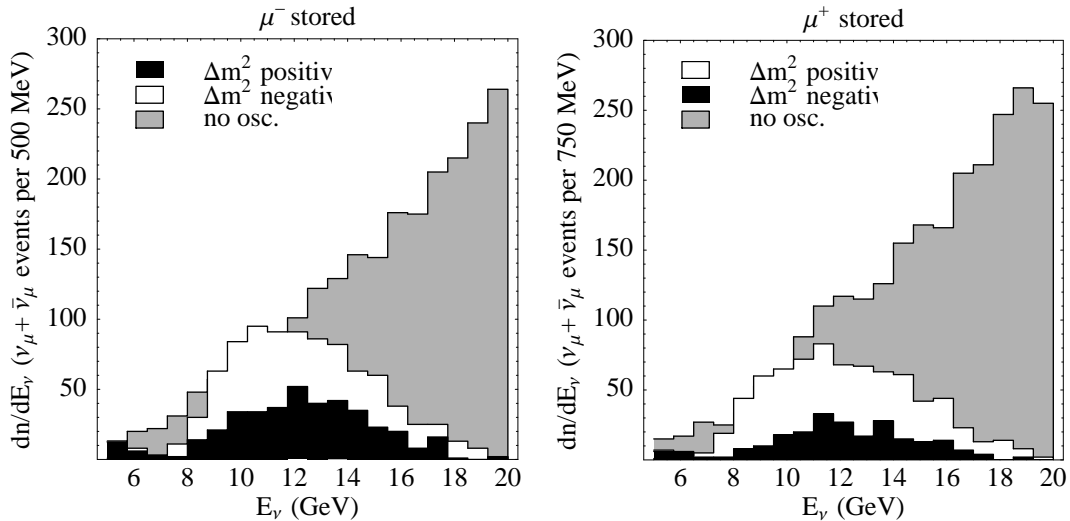


Figure 4: Spectral distribution of the muon rates $\nu_\mu + \bar{\nu}_\mu$ according to fig. 3 for $\sin^2 2\theta_{13} = 0.1$. The left plot was done for negative stored muons, the right plot for positive muons. We use 20 energy bins over the range from 5 GeV to 20 GeV.

could be used as a basis for cuts in order to amplify the signal relative to the oscillation signal. We will fit therefore in the following differential event rate spectra of data simulated with certain initial parameters and with statistical noise added. We will show how well these parameters can be re-extracted in an appropriate statistical way. We provide therefore in the next section information about the used statistical procedures and we will study then in more detail the statistical significance of the matter effects in the appearance channels, disappearance channels and combinations thereof. We focus on the potential to extract θ_{13} , the sign of Δm_{31}^2 and to test matter effects.

⁴For μ^- beams holds the same for a reversed sign of Δm_{31}^2 .

5 Statistical Methods and Data Evaluation

We numerically simulate data for a given parameter set $(E_\mu, \Delta m_{31}^2, \sin^2 2\theta_{23}, \sin^2 2\theta_{13})$ and add Poisson distributed fluctuations to the energy bins. The analysis of these “data” is done according to the procedure proposed by the Particle Data Book [26] for Poisson distributed quantities. Confidence levels (CL) are calculated by using

$$\chi^2 = \sum_{i=1}^n \left(2 [n_i^{\text{th}} - n_i^{\text{obs}}] + 2n_i^{\text{obs}} \log \frac{n_i^{\text{obs}}}{n_i^{\text{th}}} \right) . \quad (17)$$

We assume symmetric operation of the neutrino factory in both polarities, i.e. μ^+ and μ^- beams together with a detector such that $N_{\mu^+} N_{\text{kT}\epsilon_\mu} = N_{\mu^-} N_{\text{kT}\epsilon_\mu} = 2 \cdot 10^{21}$. The total χ^2 is given by

$$\chi^2 = \chi_{\mu^+}^2 + \chi_{\mu^-}^2 . \quad (18)$$

If there is no charge identification then $n_i = (n_{\mu^+})_i + (n_{\mu^-})_i$ is the total (indistinguishable) number of ν_μ and $\bar{\nu}_\mu$ induced muon events in the i -th energy bin and *obs* and *th* label the observed (i.e. simulated) and theoretical predicted muon event rates. With charge separation we calculate $\chi_{\mu^\pm}^2$ separately for neutrinos and antineutrinos and use the sum

$$\chi^2 = \chi_{\mu^-, \nu}^2 + \chi_{\mu^-, \bar{\nu}}^2 + \chi_{\mu^+, \nu}^2 + \chi_{\mu^+, \bar{\nu}}^2 . \quad (19)$$

Next χ^2 is minimized as usual with respect to the parameters shown in the plots. We subtract the minimum value of χ^2 and define confidence levels according to the values of

$$\Delta\chi^2 = \chi^2 - \chi_{\text{min}}^2 \quad (20)$$

This $\Delta\chi^2$ obeys a χ^2 distribution for k degrees of freedom (i.e. the number of parameters fitted). The value of $\Delta\chi_{CL}^2$ which corresponds to a given confidence level CL is given by:

$$CL = \int_0^{\Delta\chi_{CL}^2} \frac{x^{\frac{k}{2}-1} e^{-\frac{x}{2}}}{2^{\frac{k}{2}} \Gamma(\frac{k}{2})} dx \quad (21)$$

For two degrees of freedom ($1\sigma, 2\sigma, 3\sigma$) corresponds to $CL = (68.3\%, 95.5\%, 99.7\%)$ and to $\Delta\chi_{CL}^2 = (2.3, 6.2, 11.8)$, as usual.

We use in our analysis for the interval between 5 GeV and 20 GeV a total of 20 bins. We checked that the statistical significance of the results does not change much by changing the number of bins, as long as one has enough bins to describe the spectral information sufficiently. Finer binning does thus not improve the significance due to the statistical limitation by fluctuations. In this sense it is best to use around 20 energy bins which should not be a problem with the usual energy resolution of detectors.

6 Results

As outlined above, we simulate a measurement with certain input parameters including statistical fluctuations for a given sign of Δm_{31}^2 . Then we try to fit this dataset, i.e. we re-extract the input parameters both with the right and the wrong sign of Δm_{31}^2 . Instead of a

global fit to all parameters one can first fit the magnitude of $|\Delta m_{31}^2|$ and $\sin^2 2\theta_{23}$ with good precision (a few percent [3]) by analyzing the muon spectrum for the dominant $\nu_\mu \rightarrow \nu_\mu$ and $\bar{\nu}_\mu \rightarrow \bar{\nu}_\mu$ disappearance oscillation⁵. The following plots assume that this analysis is done and we analyze then with $\sin^2 2\theta_{23}$ fixed the matter induced effects and extract $\sin^2 2\theta_{13}$ and the sign of Δm_{31}^2 . We will see that this works very well if the mixing angle θ_{13} is not too small. The value of $\Delta\chi^2$ for the wrong sign of Δm_{31}^2 will tell us the confidence level at which we can reject the incorrect sign of Δm_{31}^2 . For the right sign we can calculate confidence level contour lines from which we can read off the sensitivity for the determination of the relevant oscillation parameters. The $\Delta\chi^2$ values printed in the following figs. 5 - 7 next to the CL contour lines are for the wrong sign of Δm_{31}^2 relative to the best fit with the correct sign of Δm_{31}^2 . This are in figure 5 the values of the global minima with the wrong sign. In the other two figures we used the information on $|\Delta m_{31}^2|$ from the fit in the $\sin^2 2\theta_{23}$ - $|\Delta m_{31}^2|$ plane to reject Δm_{31}^2 values which are inconsistent with the $|\Delta m_{31}^2|$ value obtained before. We therefore restrict the fit for the wrong sign of Δm_{31}^2 to the local minimum of χ^2 in the neighborhood of the best fit of $|\Delta m_{31}^2|$.

Fig. 5 shows the 1σ and 2σ contour lines of the right sign fit for different $|\Delta m_{31}^2|$ and different θ_{13} in the case with no charge separation (i.e. muons of either charge coming from ν_μ or $\bar{\nu}_\mu$). With decreasing θ_{13} , the precision in the determination of $\sin^2 2\theta_{13}$ gets worse, but this method allows to determine $\sin^2 2\theta_{13}$ already down to values of order $\mathcal{O}(10^{-2})$ (see also fig. 8 and discussion). Since the fitted spectrum includes the dominant disappearance channel, quite a good precision can be obtained also for $|\Delta m_{31}^2|$.

Charge separation capabilities improve the sensitivity for $\sin^2 2\theta_{13}$. This is shown in fig. 6, which shows the results of a fit to the appearance channel only (wrong sign muon events). In this case, which does not include the disappearance events in the analysis, one loses of course precision in finding the right value of $|\Delta m_{31}^2|$. The precision for $|\Delta m_{31}^2|$ can of course be improved in this case by a separate analysis of the disappearance spectrum [6]. Fig. 6 shows that charge identification improves the precision in the determination of $\sin^2 2\theta_{13}$ for small values of $\sin^2 2\theta_{13}$ and the sensitivity will go down to values of order $\mathcal{O}(10^{-3} - 10^{-4})$. Note, however, that for not too small mixing angles $\sin^2 2\theta_{13}$ of about one magnitude below the current CHOOZ constraint, we find that the sum-rates without charge identification provide at least an equally well suited possibility to extract the value of $\sin^2 2\theta_{13}$. The determination of the sign of Δm_{31}^2 is always better in the appearance channel, but note that the sum-rates give also quite good confidence levels for not too small mixing angles θ_{13} .

If charge identification is available then there is however an even better strategy by combining all available information, i.e. a global fit to the matter effects of both the appearance and disappearance channels. The results of this fit are shown in fig. 7. Now high precision is obtained both for θ_{13} and in the determination of Δm_{31}^2 .

The presented fits were all done with a fixed mixing angle $\sin^2 2\theta_{23} = 1$ and it is in principle no problem to perform a full three parameter fit for Δm_{31}^2 , $\sin^2 2\theta_{13}$ and $\sin^2 2\theta_{23}$. The contour lines of our fits have to be extended into the third $\sin^2 2\theta_{23}$ dimension and the precision is roughly given by the results in ref. [6]. As explained above in the analytic

⁵One could combine the differential event rates coming from the μ^+ and μ^- beams, weighted to correct for the cross section differences, such that the matter dependence is almost removed. This allows a determination of $|\Delta m_{31}^2|$ and $\sin^2 2\theta_{23}$ which is essentially independent of the sign of Δm_{31}^2 and $\sin^2 2\theta_{13}$.

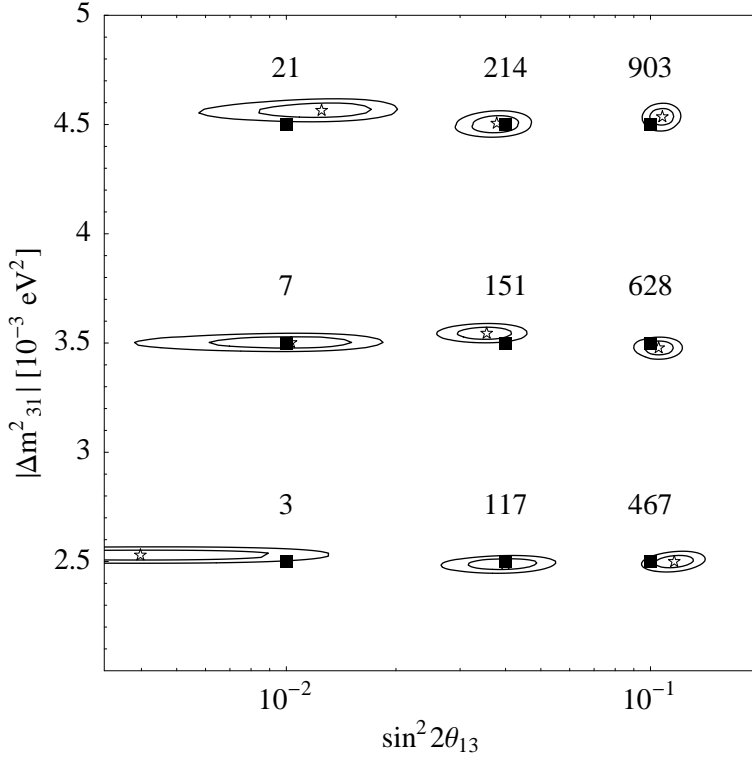


Figure 5: Fit to the muon neutrino spectrum without charge identification (*i.e.* the sum of unoscillated ($\nu_\mu \rightarrow \nu_\mu$) and oscillated ($\bar{\nu}_e \rightarrow \bar{\nu}_\mu$) muon neutrinos) for $\Delta m_{31}^2 > 0$ at a baseline of 7332 km. Shown are the 1σ and 2σ contours. The rectangles denote the parameter pair for which the data were generated and the stars denote the obtained best fit. The numbers printed next to each case are the values of χ^2 per 2 d.o.f for the best fit with the wrong sign of Δm_{31}^2 .

discussion, there is no need to include further parameters like Δm_{21}^2 and the CP-phase δ as long as the LMA MSW solution is not realized with a value of Δm_{21}^2 close to its current upper limit of order $\mathcal{O}(10^{-4})$ [27, 25, 28, 29, 30, 31]. If this scenario were however realized, such that CP-effects play a role, then this would be another reason to go for measurements based on matter effects to largest possible baselines like 7332 km. The point is that the relative magnitude of effects coming from $\Delta m_{21}^2 \neq 0$ and δ decrease for longer baselines [25]. Such a scenario would however also enable a measurement of the CP violating effects at shorter baselines such that two experiments, one at a large baseline (for matter effects) and another a shorter baseline (say 2800 km for CP violating effects) would be ideal.

Fig. 8 shows finally the region of the Δm_{31}^2 - $\sin^2 2\theta_{13}$ parameter space where a determination of the sign of Δm_{31}^2 will be possible. Shown are the 1σ , 2σ and 3σ contour lines of a fit with the wrong sign of Δm_{31}^2 for positive Δm_{31}^2 (left plot) and negative Δm_{31}^2 (right plot). For positive Δm_{31}^2 the cross section favored neutrino channels show resonant matter effects whereas for negative Δm_{31}^2 the cross section disfavored antineutrino channels are resonant. Thus in the case of positive Δm_{31}^2 the confidence level at which the wrong sign can be excluded is slightly better. The dotted lines show the limits which can be obtained with

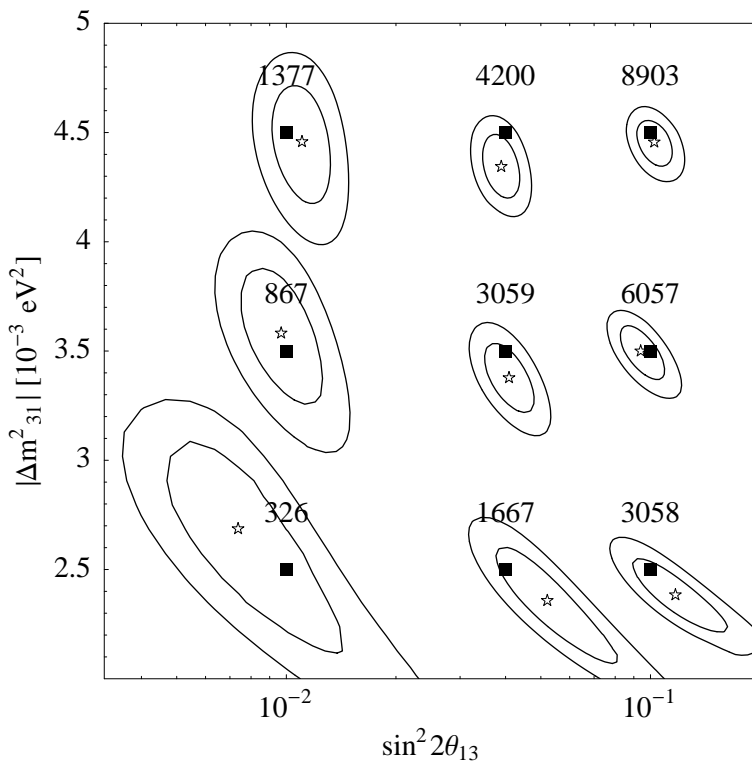


Figure 6: Fit to the muon neutrino appearance ($\bar{\nu}_e \rightarrow \bar{\nu}_\mu$) spectrum with charge identification for $\Delta m_{31}^2 > 0$ at a baseline of 7332 km. Shown are the 1σ and 2σ contour lines. The black rectangles denote the parameter pair for which the data were generated and the stars denote the best fit. The numbers next to the contour lines are χ^2 per 2 d.o.f values for the local minima of the same parameters, but with the wrong sign of Δm_{31}^2 . The global minimum is excluded in this case because its Δm_{31}^2 is already excluded.

charge identification from the spectral data of the appearance channels. The solid lines are based on an analysis of the combined channels without charge identification. Charge separation capabilities which allow to use the statistically favored pure appearance channel are thus very important if $\sin^2 2\theta_{13}$ turns out to be smaller than $\simeq 10^{-2}$.

From this discussion it seems clear that one should include charge identification. But there are other issues which may turn out to be equally important as the discussion of statistics and rates which was presented here. If, for example, right sign muon rejection (i.e. charge identification) turns out to be less good than hoped, or if there were background issues which make it hard or impossible to isolate correctly the wrong sign $\nu_e \rightarrow \nu_\mu$ muon signal then our proposed method without charge identification should still work. Many of these issues are still under discussion [17, 18, 19]. To illustrate the requirements for charge identification assume 100,000 muon events in a detector (which corresponds roughly to a baseline of 3000 km and a beam energy of 50 GeV with the usual beam and detector parameters) and right sign charge rejection of 10^{-4} , which would lead in average to 10 background events in the appearance channel which limits the ultimate sensitivity to $\sin^2 2\theta_{13}$ considerably. The problem can not be overcome by increasing statistics (i.e. by increasing $N_{\mu^\pm} N_{\text{KT}\epsilon_\mu}$) since the

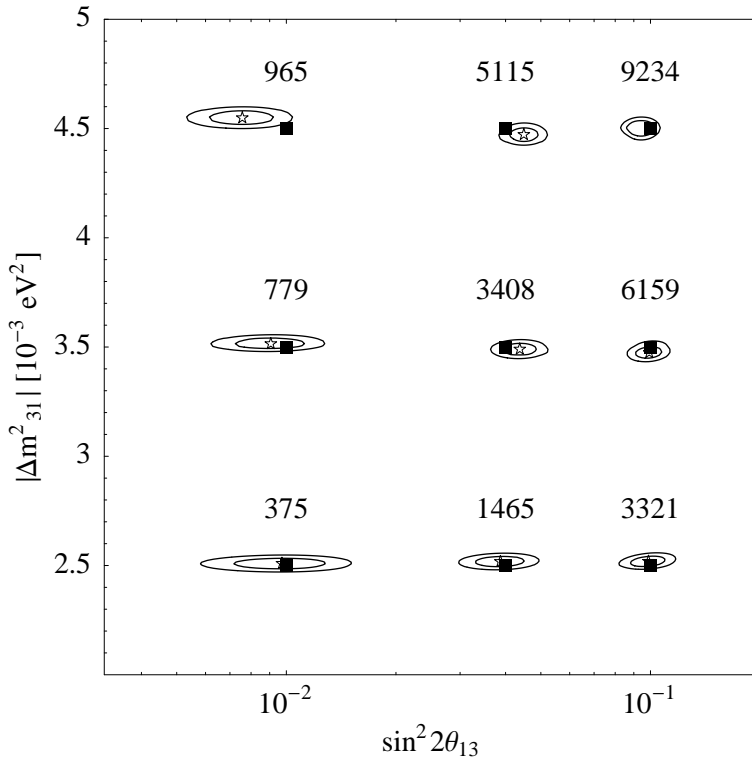


Figure 7: *Fit to the muon neutrino spectrum with charge identification (i.e. $\nu_\mu \rightarrow \nu_\mu$ and $\bar{\nu}_e \rightarrow \bar{\nu}_\mu$ channels separated) for $\Delta m_{31}^2 > 0$ at a baseline of 7332 km. Shown are the 1σ and 2σ contours. The rectangles denote the parameter pairs for which the data were generated and the stars denote the best fits. The numbers printed next to the contour lines are the local minima of χ^2 per 2 d.o.f with the same parameters, but the wrong sign of Δm_{31}^2 . The global minimum is excluded because its Δm_{31}^2 value is out of range.*

signal to background ratio stays constant. Any real detector may thus be limited by its right sign charge rejection capability and the number of right sign muons. This is also connected to the question which baseline should be used. The amount of background is typically directly proportional to the disappearance rates. This would favour larger baselines, since the disappearance rates drop faster than the appearance rates, improving the signal to background ratio for longer baselines. The decreased statistics in the $\sin^2 2\theta_{23}$ and $|\Delta m_{31}^2|$ determination (with a precision of the order of a few percent) is not a problem since this will be limited by systematics and not statistics, even for the longest baselines.

7 Conclusions

We studied in this paper different possibilities to use matter effects to determine the value and the sign of Δm_{31}^2 and the magnitude of $\sin^2 2\theta_{13}$ in very long baseline experiments with neutrino factories. The analysis rests on the detection of muons coming from muon-neutrinos or antineutrinos and we distinguish detectors with and without right sign muon charge

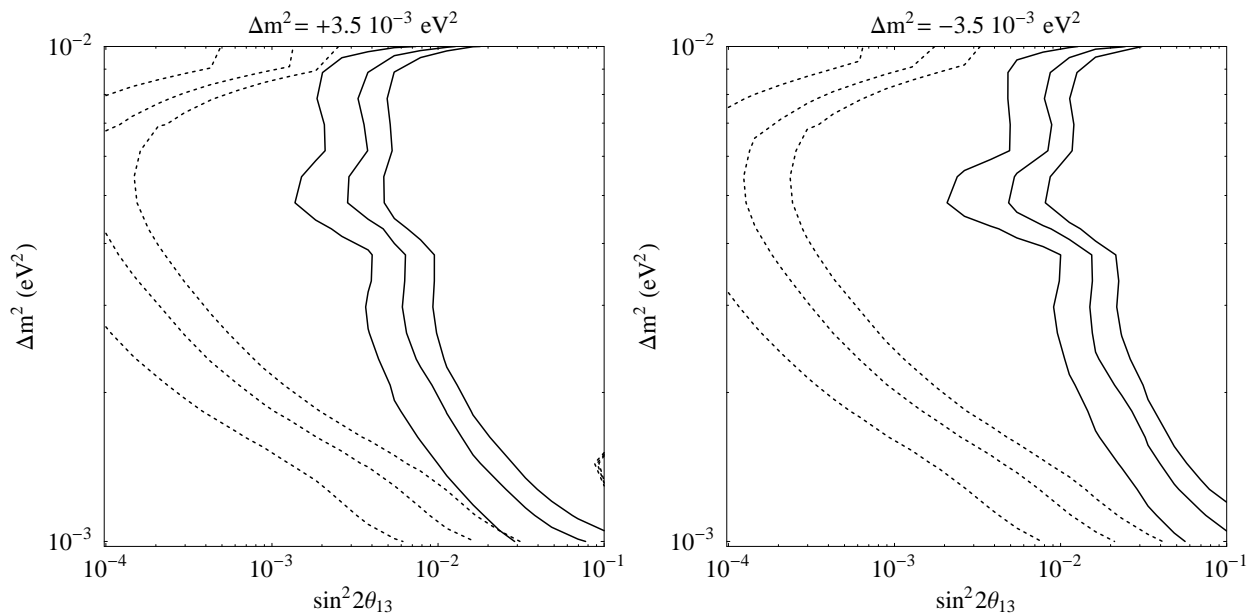


Figure 8: Sensitivity to the sign of Δm^2 . Shown are the 1σ , 2σ and 3σ contour lines of a fit with the wrong sign of Δm^2 . The dotted lines are based on spectral data from the appearance channel only. The solid lines use the combined data from the appearance and disappearance channels without separation of right and wrong sign muons. (7332 km, $|\Delta m_{31}^2| = 3.5 \cdot 10^{-3} \text{ eV}^2$ and $N_{\mu^\pm} N_{kT} \epsilon_\mu = 2 \cdot 10^{21}$).

rejection capabilities. This may be important since the $\nu_e \rightarrow \nu_\mu$ and $\bar{\nu}_e \rightarrow \bar{\nu}_\mu$ appearance channels have rather small total event rates and they require very good efficiencies for the detection of wrong sign muon events. Backgrounds due to charge misidentification play an especially important role for very small $\sin^2 2\theta_{13}$ and at too short baselines, where the dominant non-oscillated neutrino rates are high. Studies of charge identification capabilities are presently performed [8, 17, 18, 19].

We discussed the relevant appearance and disappearance rates analytically and we performed numerical simulations which were used to test the parameter extraction from event rates in a statistical reliable way. Our results show for large baselines like 7332 km that there are matter effects of comparable size in the event rates in the $\nu_e \rightarrow \nu_\mu$ and $\bar{\nu}_e \rightarrow \bar{\nu}_\mu$ appearance and in the $\nu_\mu \rightarrow \nu_\mu$ and $\bar{\nu}_\mu \rightarrow \bar{\nu}_\mu$ disappearance channels. Matter effects in the disappearance channels alone are however statistically somewhat disfavored, since they have to be extracted from the relatively large amount of un-oscillated events. Without sufficient charge identification capabilities there is however still the advantage that matter effects in the combined muon rates resulting from ν_μ and $\bar{\nu}_\mu$, i.e. generated from the combined appearance and disappearance channels, add in a constructive way. This allows a determination of $\sin^2 2\theta_{13}$ and the sign of Δm_{31}^2 even without charge identification down to mixings $\sin^2 2\theta_{13} = 10^{-2}$ and with a precision comparable to the appearance channels with perfect charge separation. This new method allows thus to measure or limit the mixing $\sin^2 2\theta_{13}$ roughly one order of magnitude below the present CHOOZ limit. With charge identification one can get better results from the appearance channels alone. We pointed however out

that with charge identification the best results can be obtained by combining all information from the appearance and disappearance channels. In this case one can measure or limit the mixing down to $\sin^2 2\theta_{13} \simeq 10^{-4}$. We gave exclusion plots which display the parameter range where a determination of the sign of the mass squared difference Δm_{31}^2 will be possible.

Our results were obtained in the approximation where Δm_{21}^2 corrections are negligible which allowed an analytic description. In the limit $\Delta m_{21}^2 = 0$ CP violating effects drop out and matter effects can be understood in an effective two neutrino scheme which is inserted into the full three neutrino oscillation formulae. It should however be stressed that there will be sizable corrections to this picture for shorter baselines if Δm_{21}^2 is at its upper limit. In this case the fit of Δm_{31}^2 , $\sin^2 2\theta_{13}$ and $\sin^2 2\theta_{23}$ had to include in addition Δm_{21}^2 and the CP-phase δ . These extra $\Delta m_{21}^2 \neq 0$ effects become however much smaller for longer baselines, such that larger baselines are safer without losing detection capabilities for matter effects. We did not discuss in more detail baseline and beam energy optimization since it depends on the preferred quantities, improvements on the knowledge of some parameters and the number of different baselines (i.e. beams and experiments) available. We mentioned however that a too short baseline could potentially also be dangerous if one neglects imperfect charge separation and other backgrounds. It seems therefore that larger baselines above 3000 km are also preferred from this point of view. We restricted our analysis therefore to a baseline of 7332 km which is very well suited for our study. We used a muon beam energy of 20 GeV, since it gives a spectrum centered around the resonance energy of matter effects in earth and which seems to be preferred by recent studies of entry level neutrino factories [16].

Acknowledgments: We wish to thank S.T. Petcov and A. Romanino for discussions on subjects related to this work.

References

- [1] S. Geer, Phys. Rev. **D57** (1998) 6989, (E) *ibid.* **D59** (1999) 039903.
- [2] A. De Rujula, M.B. Gavela and P. Hernandez, Nucl. Phys. **B547** (1999) 21.
- [3] V. Barger, S. Geer and K. Whisnant, e-Print Archive: hep-ph/9906487.
- [4] M. Campanelli, A. Bueno and A. Rubbia, e-Print Archive: hep-ph/9905240.
- [5] Nufact '99 Workshop, July 5–9th, Lyon. See e.g. the Summary of Detector/Neutrino Beam Parameters by D. Harris, <http://lyopsr.in2p3.fr/nufact99/talks/harrisconc.ps.gz>.
- [6] V. Barger, S. Geer, R. Raja and K. Whisnant, e-Print Archive: hep-ph/9911524.
- [7] V. Barger, G. Geer, R. Raja, K. Whisnant, e-print Archive: hep-ph/0003184.
- [8] A. Cervera, A. Donini, M.B. Gavela, J.J. Gomez Cadenas, P. Hernandez, O. Mena and S. Rigolin, e-Print Archive: hep-ph/0002108.
- [9] S.P. Mikheyev and A.Yu. Smirnov, Yad. Fiz. **42** (1985) 1441; Sov. J. Nucl. Phys. **42** (1985) 913;
S.P. Mikheyev and A.Yu. Smirnov, Nuovo Cimento **C9** (1986) 17;
L. Wolfenstein, Phys. Rev. D **17** (1978) 2369; **20** (1979) 2634.
- [10] S.M. Bilenky, J. Hosek and S.T. Petcov, Phys. Lett. **B94** (1980) 495;
P. Langacker, S.T. Petcov, G. Steigman and S. Toshev, Nucl. Phys. **B282** (1987) 589.
- [11] M. Apollonio et al. (CHOOZ collaboration), e-Print Archive: hep-ex/9907037.
- [12] F.D. Stacey, *Physics of the Earth*, 2nd edition, John Wiley and Sons, New York, 1977.
- [13] A.D. Dziewonski and D.L. Anderson, Phys. Earth Planet. Interiors **25** (1981) 297.
- [14] I. Mocioiu and R. Shrock, e-Print Archive: hep-ph/9910554 and e-Print Archive: hep-ph/0002149.
- [15] M. Freund and T. Ohlsson, e-Print Archive: hep-ph/9909501.
- [16] S. Geer for the Neutrino Factory Physics Study Group,
Talk presented at the FNAL Two-Day Meeting: 17-18 th February, 2000
http://www.fnal.gov/projects/muon_collider/nu/study/study.html
- [17] D. Harris for the Neutrino Factory Physics Study Group,
Talk presented at the FNAL Two-Day Meeting: 17-18 th February, 2000
http://www.fnal.gov/projects/muon_collider/nu/study/study.html
- [18] P. Spentzouris for the Neutrino Factory Physics Study Group,
Talk presented at the FNAL Two-Day Meeting: 17-18 th February, 2000
http://www.fnal.gov/projects/muon_collider/nu/study/study.html

- [19] K. McFarland for the Neutrino Factory Physics Study Group,
Talk presented at the FNAL Two-Day Meeting: 17-18 th February, 2000
http://www.fnal.gov/projects/muon_collider/nu/study/study.html
- [20] LSND Collaboration, Nucl. Phys. Proc. Suppl. **77** (1999) 207.
- [21] Super-Kamiokande Collaboration, Nucl. Phys. Proc. Suppl. **76** (1999) 425.
- [22] GALLEX and GNO Collaborations, Nucl. Phys. Proc. Suppl. **77** (1999) 26.
- [23] K. Scholberg, for the Super-Kamiokande Collab., e-Print Archive: hep-ex/9905016.
- [24] G.L. Fogli, E. Lisi, D. Montanino and A. Palazzo, e-Print Archive: hep-ph/9912231 and 9910387; M. Nakahata, in *TAUP'99*, VIth International Workshop on Topics in Astroparticle and Underground Physics, September 6 - 10, 1999, Paris, France, to appear (transparanceis available at <http://taup99.in2p3.fr/TAUP99/>).
- [25] M. Freund, M. Lindner, S.T. Petcov and A. Romanino, e-Print Archive: hep-ph/9912457.
- [26] C. Caso et al., The European Physical Journal **C3** (1998) 1, and 1999 off-year partial update for the 2000 edition available on the Particle Data Group WWW pages (URL: <http://pdg.lbl.gov/>).
- [27] K. Dick, M. Freund, M. Lindner and A. Romanino, Nucl. Phys. **B562** (1999) 29.
- [28] A. Romanino, e-Print Archive: hep-ph/9909425, to be published in Nucl. Phys **B**.
- [29] A. Donini, M.B. Gavela, P. Hernandez and S. Rigolin, e-Print Archive: hep-ph/9909254.
- [30] P.K. Kuo and J. Pantaleone, Phys. Lett. **B198** (1987) 406.
- [31] M. Koike and J. Sato, e-Print Archive: hep-ph/9909469 and hep-ph/9911258.